6

Biomimetic Materials Synthesis from Ferritin-Related, Cage-Shaped Proteins

Pierpaolo Ceci[1], Veronica Morea[1], Manuela Fornara[1],
Giuliano Bellapadrona[2], Elisabetta Falvo[3] and Andrea Ilari[1]
[1]*C.N.R. Institute of Molecular Biology and Pathology, Rome*
[2]*Department of Materials and Interfaces, Weizmann Institute of Science, Rehovot*
[3]*Regina Elena Cancer Institute, Pharmacokinetic/Pharmacogenomic Unit, Rome*
[1,3]*Italy*
[2]*Israel*

1. Introduction

Protein cages are characterized by a quaternary structure consisting in an assembly of multiple subunits endowed with highly similar three-dimensional structures. These assemblies enclose hollow spaces that can be used as ideal templates for the encapsulation of nano-material cargos. Indeed, the uniformity of the quaternary structure guarantees the attainment of nanoparticles (NPs) that are highly homogeneous in both size and shape, and the interior of the cage provides an isolated environment, shielded from bulk solution, where chemical reactions can take place. The protein surface is decorated by diverse chemical groups (*i.e.*, primary amines, carboxylates, thiols) that can be genetically and/or chemically manipulated in order to confer specific functionalities to the nano-cage. Further advantages of protein cages include their usually remarkable stability, which is generally higher than that of liposome-based molecules, and high solubility in water, as well as the fact that protein-encapsulated NPs can be produced in industrial strains on large-scale, high yield (grams or even kilograms) and low cost. Finally, the determination of the three-dimensional structures of protein-cages at the atomic level has provided relevant information to understand the biomineralization processes and design protein variants aimed at the creation of new functional biomaterials.

Members of the ferritin family, including ferritins and **D**NA-binding **p**roteins from **s**tarved cells (Dps), are among the most widely studied cage-like proteins. The unique template structures of these proteins have been used for the synthesis of a variety of new, non physiological mineral cores within the protein shell.

Ferritins are formed by 24 subunits assembled with octahedral (432) symmetry, whereas Dps are formed by 12 subunits assembled with a 23 rotational tetrahedral symmetry. Despite their different size and architecture, both ferritins and Dps assemblies have a spherical shape enclosing an inner cavity where iron is conserved in a non-toxic and bioavailable form. Both these molecules play a key role in cellular protection by maintaining iron homeostasis. In addition, Dps protect DNA from oxidative damage by a chemical

mechanism, involving the consumption of hydrogen peroxide produced by the oxidative metabolism, and by a physical mechanism, consisting in DNA condensation and shielding. The shells of ferritins and Dps are traversed by pores allowing the passage of ions and small molecules. In particular, hydrophilic pores, lined with negatively charged residues, are involved in the uptake of Fe(II) ions, which are guided through the pores by a negative electrostatic charge (**Fig. 1**). After entering the pores, reduced iron atoms reach specific catalytic sites, named ferroxidase centres, where Fe(II) is oxidized to Fe(III) either by molecular oxygen (in ferritins) or hydrogen peroxide (in Dps). Fe(III) then moves to the protein cavity and binds to specific nucleation sites where it forms ferrihydrite (Fe(III)OOH) clusters, which grow until a single core (NP) of up to 500 iron atoms in Dps and 4000-5000 iron atoms in ferritins is formed.

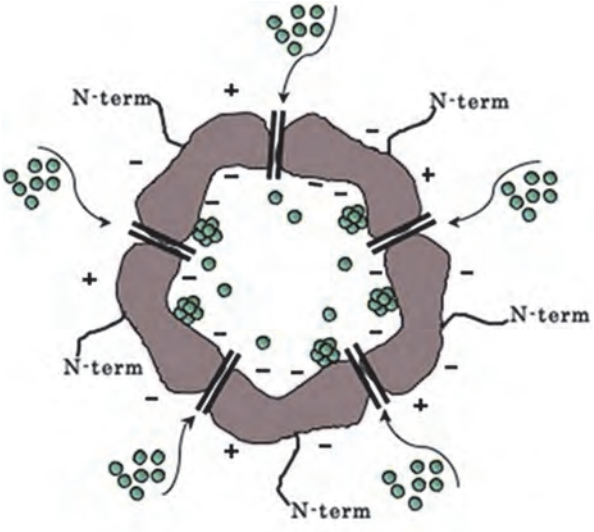

Fig. 1. Schematic illustration of ferritin. A negative electrostatic charge facilitates the passage of ions and small molecules through the pores traversing the protein shell. The quaternary structure consists of 24 subunits whose amino-termini (denoted with N-term) protrude from the external surface. Plus and minus signs indicate the higher concentration of negative charges on the internal surface with respect to the external one

A different mechanism of biomineralization is represented by the formation of specific intracellular structures called magnetosomes, which allow magnetotactic bacteria to navigate along geomagnetic fields. Magnetosomes originate from invaginations of the inner membrane and contain magnetite (iron oxide) or greigite (iron sulfide) nanoparticles that can reach dimensions up to 70 nm in diameter (Mann et al., 1990). Magnetosome assembly and function are governed by several proteins (Mam A, B, C, D, E) (Grünberg et al., 2001). Commercial uses of bacterial magnetosome particles have been suggested, including magnetic targeting of pharmaceuticals and enhancement of contrast agents in magnetic resonance imaging.

In this chapter we will describe the structural properties of ferritin-like proteins, the mechanisms of metal incorporation and the use of ferritin-like proteins as size-constrained

reaction vessels. In particular, we will examine the main parameters involved in the biomineralization process, *i.e.*, the external/internal charge distribution and the number and type of metal binding/nucleation sites present inside the protein cavity. Finally, we will discuss the current and potential applications of ferritins in the fields of biomedicine, catalysis and electronics.

2. Structural and functional properties of cage-like proteins in biology: Ferritins and Dps

2.1 Iron homeostasis

Nearly all forms of life require iron. This metal commonly occurs in either the ferrous (Fe(II)) or ferric (Fe(III)) oxidation state. The wide range of the Fe(II)/Fe(III) redox potential (from approximately −500 to +600 mV, depending on the iron ligands and surrounding chemical environment) as well as the ability of iron to gain and lose electrons, thus cycling between the two oxidation states, makes iron an ideal redox catalyst in many biological processes. However, iron can also be a major problem for the cell. Firstly, Fe(III) is highly insoluble and precipitates in the cytoplasm as part of the uncharged species $Fe(OH)_3 \cdot 3(H_2O)$ (Ksp, 10^{-38}) (Aisen et al., 2001), thereby limiting the cellular concentration of free iron to 10^{-17} M at neutral pH. The reaction between Fe(II) and molecular oxygen is also a source of oxidative stress for the cell. The one electron reduction of Fe(II) by O_2 results in the formation of the superoxide radical $O_2^{\bullet -}$, which can accept another electron and two protons to produce hydrogen peroxide, H_2O_2. The superoxide radical and hydrogen peroxide are the by-products of incomplete O_2 reduction, and their balance is regulated by the enzyme superoxide dismutase (McCord & Fridovich, 1988). In addition, hydrogen peroxide can react again with Fe(II) generating hydroxyl radical species ($^{\bullet}OH$) via the Fenton reaction (1), while the $O_2^{\bullet -}$ radical can reduce ferric iron to ferrous ions (2):

$$Fe(II) + H_2O_2 \rightarrow Fe(III) + {}^{\bullet}OH + OH^- \quad (1)$$

$$O_2^{\bullet -} + Fe(III) \rightarrow O_2 + Fe(II) \quad (2)$$

The sum of these two reactions, named Haber–Weiss reaction (3), occurs in the presence of catalytic amounts of free iron ions and produces the hydroxyl anion, hydroxyl radical and O_2:

$$H_2O_2 + O_2^{\bullet -} \rightarrow OH^- + {}^{\bullet}OH + O_2 \quad (3)$$

The reactive oxygen species (ROS) involved in the Haber–Weiss reaction (*i.e.*, all the involved species with the exception of molecular oxygen) are highly toxic for the cell. In particular, hydroxyl radicals can oxidize biological macromolecules, such as DNA, proteins and lipids, and all organisms have developed strategies to store iron in a non toxic and readily bio-available form.

Iron bioavailability is extremely poor in aerobic organisms under physiologic conditions, such that iron is often a limiting nutrient for growth and virulence in bacterial pathogens (Andrews et al., 2003). In conditions of low iron availability, the metal is scavenged from the environment by efficient systems. Ferric chelators called siderophores are often secreted and internalized. Host-iron complexes, such as transferrin, lactoferrin, heme, haemoglobin, are directly used as iron sources by pathogens. Highly specific proteins transport iron

complexes and heme across the cell wall of gram-positive bacteria and the outer membrane of gram-negative bacteria. ABC transporters carry heme and iron siderophores across the cytoplasmic membrane (Braun & Hantke, 2011).

One of the means that cells have adopted to protect themselves from the potentially toxic effects of free iron and radical chemistry is represented by proteins belonging to the ferritin family, including ferritins, bacterioferritins (Bfrs) and Dps proteins.

2.2 Ferritins

Ferritins are involved in iron storage and detoxification in most living organisms from microorganisms to plants, invertebrates, and mammals (Crichton & Boelaert, 2009). They are formed by 24 similar or identical subunits assembled to form a 24mer. A non-toxic, water-soluble, yet bioavailable iron core, often consisting in a ferric oxy-hydroxide mineral, is stored within the ferritin hollow shell.

Mammalian ferritins were the first to be studied from a structural and functional point of view. Typically, they are heteropolymers composed by two types of subunits named H (heavy, predominant in heart) and L (light, predominant in liver) (Drysdale, 1976). These chains are highly similar both in sequence (~55% sequence identity) and structure, since the L- and H-chain subunits can be super-imposed with an RMSD of 0.6 Å over ~170 amino acid residues (see Table 1). Additionally, they are isostructural, meaning that they can assemble in any proportion in the 24mer.

In prokaryotes there are two types of ferritins: bacterial ferritins, closely related to mammalian ferritins, and Bfrs, characterized by the presence of up to 12 heme groups per 24mer, which do not play a role in the iron oxidation and incorporation processes (Frolow et al., 1994). Sequence analyses have revealed that the sequence identity between ferritins and Bfrs is very low, generally below 15%, but the catalytically important residues are conserved (Le Brun et al., 2010). The structural analyses discussed below demonstrate that, despite their low degree of sequence identity, ferritins and Bfrs conserve the structural features required for iron oxidation and incorporation.

2.3 Dps proteins

Dps proteins, whose prototype was discovered in *Escherichia coli* (Almiron et al., 1992), are found exclusively in prokaryotes, where they are expressed under starvation and oxidative stress conditions. Like ferritins, Dps possess iron storage and detoxification capabilities, and the three-dimensional structure of individual Dps protein subunits is very similar to that of ferritin subunits. However, their quaternary assemblies are different, in that they comprise only 12 identical subunits assembled with 23 rotational tetrahedral symmetry. Therefore, the hollow shell enclosed by Dps has a smaller volume than the ferritin one, and incorporates a 10-fold smaller number of iron atoms.

Additionally, differences between Dps proteins and ferritins concern the ferroxidase centre. This is entirely comprised within each subunit in ferritin and Bfrs, whereas it is contributed by two-fold symmetry related subunits in Dps proteins (Ilari et al., 2000). Moreover, in Dps proteins it catalyzes the oxidation of ferrous iron by hydrogen peroxide within the protein shell, thus preventing the diffusion of ROS in the cytoplasm and, consequently, damage of cellular components (Bellapadrona et al., 2010).

In addition to this chemical mechanism of protection, some Dps proteins are able to protect DNA from oxidative damage by binding DNA, thus providing it with a physical shield against the damage mediated by reactive oxygen species (ROS). Dps proteins have been shown to bind DNA by one of three mechanisms, based on the following structural features: i) presence of a long N-terminal tail rich in positively charged residues, which protrudes from the dodecameric structure, as in the prototypic Dps from *E. coli* (Grant et al., 1998); ii) presence of a C-terminal tail, also protruding from the structure and containing positively charged residues, as in *M. smegmatis* Dps; iii) presence of a positively charged protein surface, as in the Dps from *H. pylori*. The physical DNA protection activity is largely influenced by the net charge and charge distribution on the protein surface, and it has been shown to be dependent on both pH and salt concentration (Chiancone & Ceci, 2010).

2.4 Building blocks: Structural monomeric units

Comparisons between the three-dimensional structures of the H and L chains of mammalian ferritins, bacterial ferritins and Bfrs subunits have revealed a striking similarity of the monomer subunit (Crichton & Declercq, 2010).

Monomers of all these proteins are folded in a characteristic four-helical bundle, formed by four antiparallel helices (A-D), and a shorter helix on the top of them (E) **(Fig. 2A)**. The most variable part of the monomer fold is represented by the loops connecting the helices, in particular the long BC loop, which stretches along the length of the helical bundle **(Fig. 2A)**, and by the short non-helical regions at the N- and C-termini. The relative orientation of the E and D helices varies in different proteins. They form an angle of 90° in both bacterial ferritins and heme-containing Bfrs, and of about 60° in mammalian ferritins. In the quaternary structure the N-terminus, BC loop, and helices A and C face the external side of the spherical shell, while helices B and D are on the internal side.

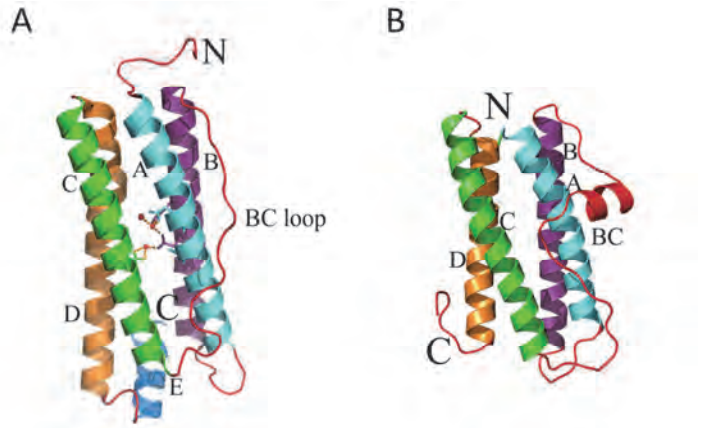

Fig. 2. Monomeric fold of ferritins and Dps. A. Human H ferritin (PDB code: 2CEI). Helices A-D forming the four-helical bundle, the E-helix and the BC loop are indicated. B. Dps from *Listeria innocua* (PDB code: 1QGH). Helices A-D forming the four-helical bundle and the BC-helix are indicated. This picture has been generated with PyMol (Delano Scientific LLC, San Carlos, LA; http://www.pymol.org).

The Dps monomer also folds into a four-antiparallel-helix bundle (**Fig. 2B**), which is almost entirely super-imposable to that of ferritins (Table 1) and Bfrs. The four helices A–D are stabilized mainly by inter-helical hydrophobic interactions. Helices B and C are connected by a long BC loop, which comprises the short BC helix. Helix E, present in the ferritin C-terminal region, is absent in Dps.

2.5 Functional components: Ferroxidase centres

Mammalian H chain ferritins are characterized by the presence of a di-iron ferroxidase centre, involved in the oxidation of Fe(II) to Fe(III). This is not present in L chains, which contain a group of conserved negatively charged residues (Glu57, Glu60, Glu61, Glu64 and Glu67, mouse L-chain numbering) directed into the inner cavity of the protein and known to be involved in the ferrihydrite nucleation process (Andrews, 2010; Drysdale, 1976; Granier et al., 2003; Nordlund & Eklund 2006).

The ferroxidase centre of H-chain ferritins has been intensively studied for several decades. However, due to instability of the iron bound form a structure of their ferroxidase centre in complex with iron is not available yet. Nevertheless, structural data on H-chains in complex with different metals, like Zn(II) and Tb(III), have been determined, based on which detailed studies on the bimetal binding centre have been performed (Lawson et al., 1989; Toussaint et al., 2007). The ferroxidase centre of mammalian H chain ferritins comprises two iron binding sites, A and B. The iron atom at site A (FeA) is ligated by one histidine, one monodentate glutamate and one bridging glutamate (His65, Glu27 and Glu62, human H chain numbering; **Fig. 3A**) **(**Santambrogio et al., 1996; Trikha et al., 1995). The iron atom at site B (FeB) is ligated by Glu62 and by two glutamate residues (Glu61 and Glu107). The conservation of the amino acid residues belonging to the ferritin ferroxidase site is highlighted by sequence alignments (Andrews et al., 1992). Although mutagenesis studies have shown that both sites A and B are important for iron uptake and oxidation, only a few ferritin structures have been determined with both sites occupied by metals**.** The structure of the H chain homopolymer in complex with Tb(III) revealed that Glu61 is able to adopt two conformations (Lawson et al., 1989). In one conformation the residue is bound to the metal at the B site and in the other it is projected towards the internal cavity (**Fig. 3A**).

The chemical environment of the ferroxidase centres of representative bacterial ferritins and Bfrs is similar to that observed in the crystal structure of recombinant human H chain ferritin (HuHFt) in complex with Zn(II) (Stillman et al., 2001). As shown in **Fig. 3B** and **3C** the ferroxidase centres of bacterial ferritins and Bfrs present many similarities with that of HuHFt. In all the ferritin monomers the iron atom in the A site is coordinated by one histidine and one glutamate residue. The iron atom in the B site is ligated by two glutamate residues and one glutamate residue bridges both metal centres.

The structures of bacterial ferritins display two main differences with respect to that of HuHFt. In *P. furiosus* ferritin (Tatur et al., 2007), whose crystals had been soaked with Fe(II), a third site (site C) has been found to be occupied by an iron atom (**Fig. 3B**) and the iron at the B site is coordinated by Glu130 as an additional ligand.

The ferroxidase centre of Bfrs displays major differences with respect to that of HuHFt and bacterial ferritins. Although the structure of the first Bfr was reported in 1994, the first iron-bound structure (*D. desulfuricans* Bfr) was described several years later (Romão et al., 2000).

Fig. 3C depicts the ferroxidase centre of the Bfr from *E. coli* (Crow et al., 2009), similar to that of Bfr from *D. desulfuricans*, which was obtained by soaking the protein crystals with a solution containing Fe(II). In this structure, the water molecule coordinating FeA in HuHFt is substituted by Glu127, which bridges the metal sites A and B. Moreover, FeB is coordinated by His130, which substitutes Glu130 present in bacterial ferritins.

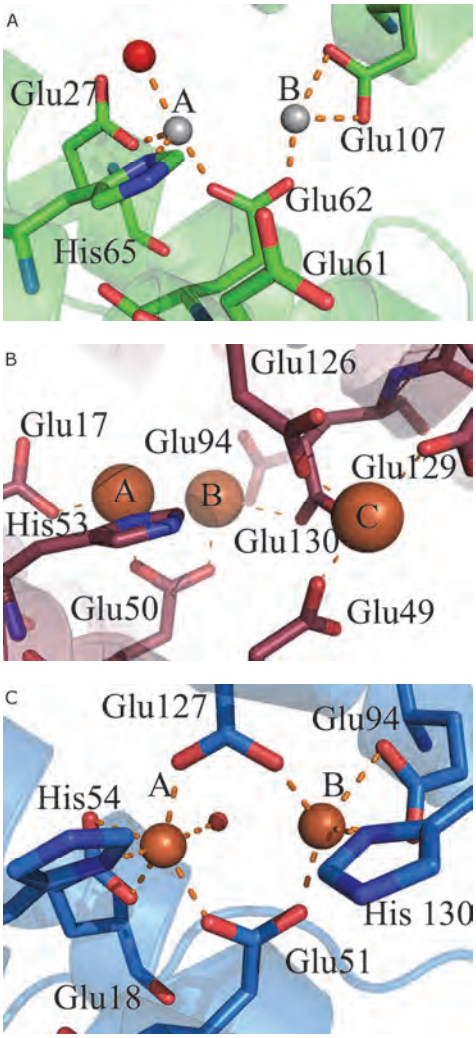

Fig. 3. Ferroxidase centre in ferritins. A. Human H chain ferritin (PDB code: 2CEI). B. *Pyrococcus furiosus* bacterial ferritin (PDB code: 2JD7). C. *E. coli* Bfr (PDB code: 3E1M). Residues are shown as sticks and coloured according to atom type: N, blue; O, red; C, green, salmon and light blue in panels A, B and C, respectively. Zn(II) atoms and the oxygen atom of a coordinated water molecule in panel A, and Fe(III) atoms in panels B and C are shown as spheres and coloured grey, red and orange, respectively. The picture was generated using PyMol

In all known ferritins and Bfrs the ferroxidase centres are embedded within each of the four-helical bundle monomers. Conversely, the functional centres of Dps proteins are located at the interface of each pair of 2-fold symmetry-related subunits (**Fig. 4A**), both of which provide the iron ligands. In particular, in the X-ray crystal structure of *L. innocua* Dps (Ilari et al., 2000), two histidine residues (H31 and H43) are provided by one subunit and two carboxylate ligands (D58 and E62) by the symmetry-related subunit within the dimer (**Fig. 4B**). These ferroxidase centre ligands are conserved in all Dps with the only known exception of *T. elongatus* DpsA, where His78 replaces the canonical aspartate (D58, *Listeria* numbering) (Alaleona et al., 2010).

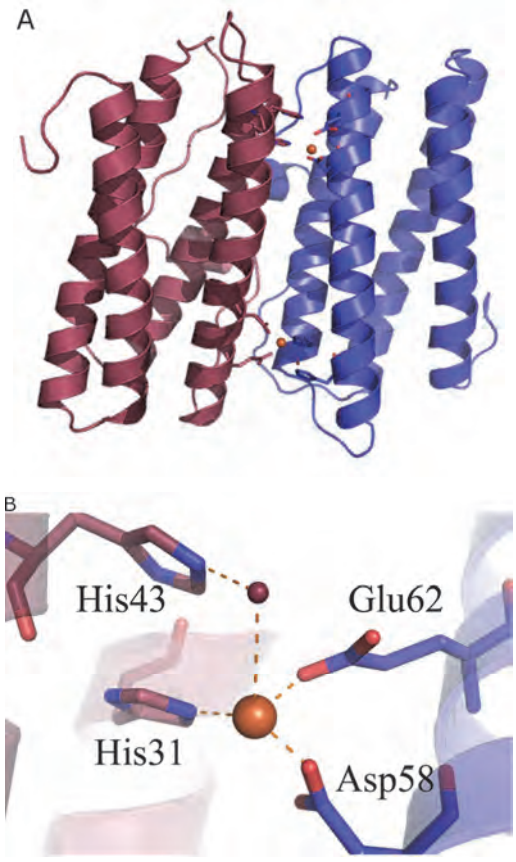

Fig. 4. Ferroxidase centre in Dps proteins. A. Two ferroxidase centres are present at the dimeric interface of the Dps from *Listeria innocua* (*Li*Dps) (PDB code: 1QGH). The 2-fold symmetry-related subunits are coloured dark red and blue, respectively. B. Blow up of one ferroxidase centre of *Li*Dps. Iron within the A site and the water molecule at the B site are indicated as spheres and coloured orange and red, respectively. Residues involved in iron or water coordination are shown as sticks and coloured according to atom type: N, blue; O, red; C, dark red (histidines from one subunit) or blue (acidic residues from the symmetry-related subunit within the dimer).

The occupancy of the two metal binding sites with iron varies significantly in the known crystal structures. In *L. innocua* Dps the ferroxidase centre contains one iron and one water molecule, which lies at about 3 Å from the iron. It has been proposed that this water molecule may be replaced by a second iron atom to give rise to a canonical bimetallic ferroxidase centre (Ilari et. al., 2000). In *D. radiodurans* Dps2 and *B. brevis* Dps, both sites are occupied by Fe(III) (Cuypers et al., 2007; Ren et al., 2003). In *H. pylori* Dps, *D. radiodurans* Dps1 and *A. tumefaciens* Dps structures, only the A site contains iron whereas the B site contains a water molecule (Ceci et al., 2003; Romão et al., 2006; Zanotti et al., 2002). In *E. coli* Dps (Grant et al., 1998) and *T. elongatus* Dps both sites are occupied by two water molecules (Franceschini et al., 2006). These data indicate that the two metal binding sites A and B have different affinity for iron, and that the second metal coordination shell, formed by residues that are not directly in contact with the metal but interact with metal binding site residues, may influence the affinity for iron. As an example, the low affinity of *E. coli* Dps for iron has been ascribed to the presence of Lys48 in the second metal coordination shell, which forms a salt bridge with Asp78 in the ferroxidase centre, reducing the iron coordination propensity of this residue (Ilari et al., 2002).

All Dps proteins bind and oxidize iron at the ferroxidase centre. The only known exception is represented by DpsA from *T. elongatus*. The peculiar set of iron coordination residues of this protein, where the conserved Asp58 (*Listeria* numbering) is replaced by His78, endows the A site with a strong affinity for Zn(II) (Alaleona et al., 2010).

2.6 Complete structure: Quaternary assembly

Ferritins are formed by 24 subunits assembled to form a compact, symmetric and extremely stable apoferritin shell. This shell has the approximate geometry of an octahedron and, therefore, possesses three four-fold axes passing through the centre of two opposite faces (**Fig. 5A**), four three-fold axes passing through two opposite vertices (**Fig. 5B**) and six two-fold axes passing through the centre of two opposite edges (**Fig. 5C**).

Vertebrate ferritins present two hydrophilic pore entrances along each three-fold axis, which allow Fe(II) to enter inside the protein. These 8 pore entrances have a ~ 4 Å diameter and are lined by Asp131 and Glu134 (HuHFt numbering) from each of the three-fold symmetry related subunits (Bou-Abdallah et al., 2008). Both the mutation of these negatively charged residues and the presence of Tb(III) or Zn(II) decrease the capacity of ferritins to oxidate and incorporate iron ions (Bou-Abdallah et al., 2003; Watt et al.,1988). The pores stretching along the four-fold symmetry axes are mostly hydrophobic, with the six pore entrances lined by leucine residues. These are believed to be the major entrance route for molecular oxygen and hydrogen peroxide inside the ferritin cavity (Liu & Theil, 2005).

With respect to vertebrate ferritins, in *E. coli* ferritin and Bfr (Stillman et al., 2001), *Azotobacter vinelandii* Bfr (Liu et al., 2004) and in ferritins from the archaeal hyperthermophiles and anaerobes *Pyrococcus furiosus* (Tatur et al., 2007) and *Archaeoglobus fulgidus* (Johnson et al., 2005), the three-fold channels are less hydrophilic while the 4-fold channels are more polar and considered to be a likely route of iron entry and release.

Identical Dps subunits give rise to dodecameric shell-like assemblages characterized by 23 rotational tetrahedral symmetry. Accordingly, the Dps molecule is smaller than ferritin and this difference in size is reflected in a lower capacity to store iron (~500 versus ~4500 atoms per oligomer).

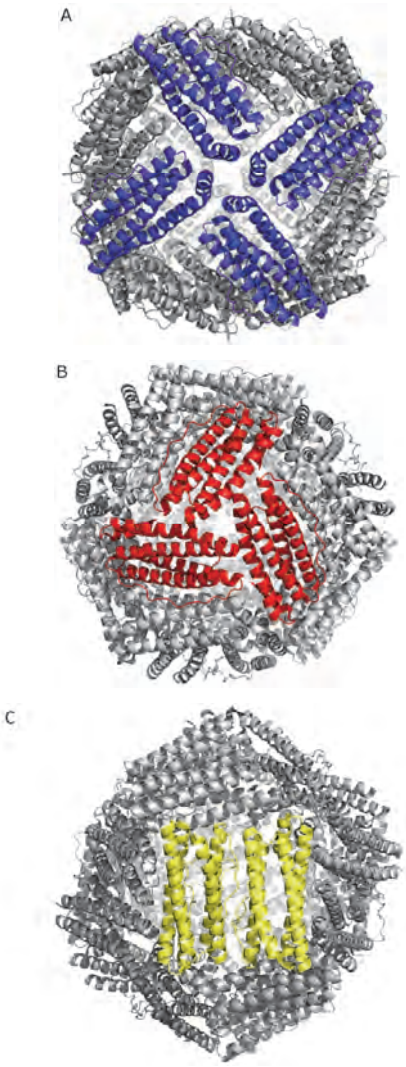

Fig. 5. Quaternary assembly of ferritin from *Pyrococcus furiosus* (PDB code: 2JD7). A. View along the four-fold axis. B. View along the three-fold axis. C. View along the two-fold axis. The subunits forming the four-, three-, and two-fold interfaces are indicated in blue, red and yellow, respectively, the other subunits are grey.

The Dps dodecamer can be viewed as an ensemble of four trimers placed at the vertices of a tetrahedron. There are three two-fold axes passing through the centres of the tetrahedron edge and the centre of the structure, and four three-fold axes passing through the vertices of the tetrahedron and the centres of the opposite face. Consequently, there are two non-equivalent environments along the three-fold axes, which have been designated "ferritin-like" (**Fig. 6A**) and "Dps-type" (**Fig. 6B**), respectively (Ilari et al., 2000). The ferritin-like interfaces resemble

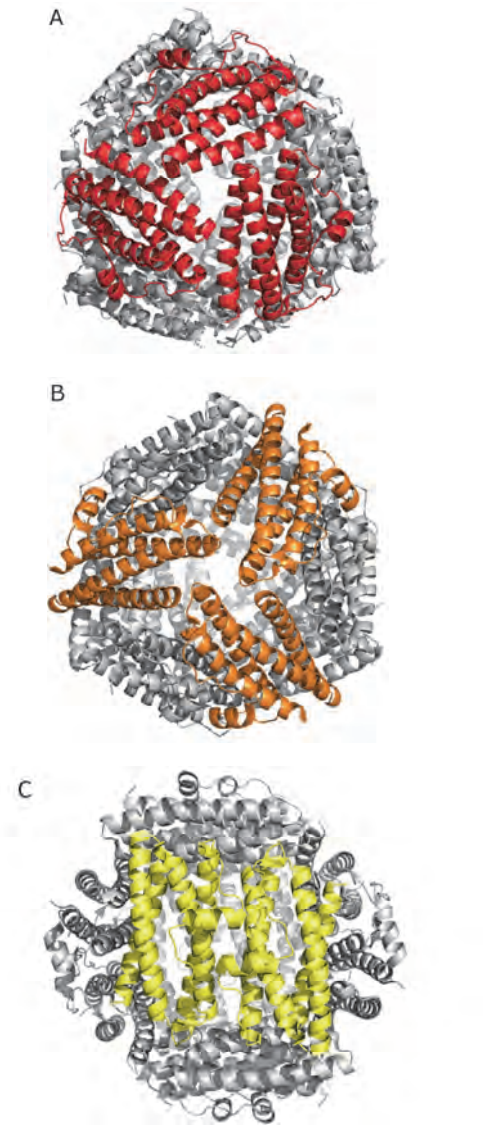

Fig. 6. Quaternary assembly of Dps from *L. innocua* (PDB code: 1QHG). A. Front-view along the three-fold axis: ferritin-like interface. B. Back-view along the three-fold axis: Dps-like interface. C. View along the two-fold axis. The monomers forming the ferritin-like and Dps-like interfaces are indicated in red and orange respectively, the subunits forming the two-fold interface are yellow and the other subunits are grey.

those formed along the three-fold symmetry axes of the ferritin oligomer. Like the ferritin pores, ferritin-like pores are rich in negatively charged aspartate and glutamate residues. These amino acid residues are the major contributors to the negative electrostatic gradient

driving iron within the protein cavity. The Dps-type interfaces are typical of these proteins and are formed by the C-terminal portions of the B and D helices (**Fig. 2A**). The Dps-type pores (external diameter 4.5 Å, **Fig. 6B**) are characterized by a marked variability in their chemical nature. The dimeric interface, comprising the ferroxidase centre, is stabilized by hydrophobic interactions involving mostly residues belonging to the short BC helices (**Fig. 6C**). The large surface area buried upon dimerization (about 1290 $Å^2$ per monomer) has been proposed to account for the stability of the dodecameric *Listeria innocua* Dps assemblage at high temperatures (≥ 70 °C) and over a wide pH range (Chiaraluce et al., 2000). The external surface of Dps proteins is generally rich in negatively charged residues, with the exception of the *H. pylori* protein, whose positively charged surface is considered to be responsible of the ability of this protein to bind DNA (Zanotti et al., 2002).

3. Iron mineralization in ferritins and Dps

3.1 The iron mineral core

Both ferritin and Dps proteins can accommodate polynuclear iron micelles within their internal cavities. Two different core types have been described: a native core, which is present in the "as purified" protein; and an *in vitro* core, which is formed after addition of iron to the apoprotein. Mammalian ferritins, as isolated, generally contain 1000-3000 atoms of iron per molecule, while Bfrs usually contain only 800-1500 iron atoms (Lewin et al., 2005). As described above, in ferritins the negatively charged channels along the 3-fold symmetry axes allow the entry of Fe(II); the ferroxidase sites located within the four-helix bundle of the so-called H-type subunits catalyze iron oxidation by O_2; and the negatively charged internal cavity allows deposition of an oxy-hydroxide core containing up to 4500 iron atoms by addition of iron to the apo- form.

A notable feature of the apoferritin moiety is its capacity to direct iron deposition towards the formation of microcrystalline structures. The characteristics of the structures formed by horse spleen and human ferritins have been elucidated by both Mossbauer spectroscopy and X-ray diffraction studies. Basically, the native microcrystalline core contains oxygen atoms packed 3 Å apart (Massover & Cowley, 1973) and iron atoms placed in spaces between oxygen layers, so that they can be coordinated either octahedrically or tetrahedrically. Although the native mineral core of eukaryotic ferritins has been traditionally described as being formed by ferrihydrite, more recent studies have revealed a polyphasic structure consisting of both ferrihydrite and other phases, including a magnetite-like phase. Ferrihydrite is less crystalline and, therefore, less stable, than other iron mineral phases. However, this phase is stable when prepared inside ferritin, highlighting the ability of biomolecules to direct and selectively stabilize specific polymorphs.

Structural information at atomic resolution for ferritin cores is lacking because preparations of iron-containing ferritins are generally poly-dispersed with respect to their metal components, even though their protein components are highly homogeneous. This has prevented determination of the structure of the mineral core within ferritins by X-ray crystallography. Poly-dispersion of the mineral core is probably due to the fact that the iron mineral can be potentially nucleated at 24 different positions relative to the crystal itself, leading to a smearing of electron density. However, other techniques that are frequently used in materials sciences have been used to clarify structural and chemical aspects of

ferritin cores. Galvez et al (2008) have used Transmission Electron Microscopy (TEM), X-ray Absorption Near Edge Spectroscopy (XANES), Electron Energy-Loss Spectroscopy (EELS), Small-Angle X-ray Scattering (SAXS), and SQUID magnetic measurements to demonstrate that the structure of the iron core of horse ferritin is formed by several iron oxide phases (ferrihydrite, magnetite, hematite), whose relative percentages vary as iron is gradually removed from the metal core. In particular, the native ferritin core mainly corresponds to a ferrihydrite phase with physiological values of 1000-2000 iron atoms, while magnetite appears to be the predominant phase when the iron content of ferritin decreases below 500 atoms. Moreover, it has been shown that the size of the iron core does not vary significantly with iron removal because iron is removed from the more chemically labile ferrihydrite core, hollowing it out, rather than from the magnetite shell.

The iron mineral cores of prokaryotic ferritins display significant variability. Bfrs cores usually have higher phosphate content with respect to eukaryotic ferritins, and appear to be largely disordered as judged by TEM analyses. X-ray absorption fine structure (EXAFS) experiments on *A. vinelandii* Bfrs with a Fe:P ratio of about 1.7:1 have shown that phosphate groups reduce the number of near-iron neighbours thus explaining the decrease in the metal core order and supporting a model for the core in which phosphate is clearly an integral constituent (Rohrer et al., 1990). Native bacterial ferritin cores have not been investigated in detail, but studies of ferritin from *H. pylori* have revealed that its core contains significant amounts of iron and phosphate with a small amount of iron oxy-hydroxide, leading to the conclusion that it has a Bfrs-like core structure (Doig et al., 1993).

The native iron core of Dps-like proteins generally contains 5-50 iron atoms, with variable proportions of phosphate (Kauko et al., 2006; Stefanini et al., 1999; Yamamoto et al., 2002). The Dps core can also contain other metals, such as Zn, Cu, Cr, Mn, Co, Ni and Mo (Yamamoto et al., 2002). *In vitro*, Dps proteins can store a maximum of approximately 450 Fe atoms per dodecamer, an amount consistent with a protein cage significantly smaller than that of mammalian apoferritin. Iron-loaded *E. coli* Dps crystals have been studied using polarized single crystal absorption micro-spectrophotometry. In these crystals iron ions are oriented with tetrahedral symmetry, with the tetrahedron centre occupied by iron ions and the vertices by oxygen atoms (Ilari et al., 2002).

Different iron nanominerals with specific magnetic properties have been created using ferritin templates, and similar approaches may be envisaged for Dps proteins as well. The ferrimagnetic iron oxide phase Fe_3O_4 has been synthesized within ferritin proteins under nitrogen flux at temperatures above 60°C, using H_2O_2 as an additional oxidant agent. These materials have been extensively characterized and can be exploited in different applications (see below).

3.2 Iron mineralization mechanisms

The most widely accepted mechanism by which iron is mineralized in ferritins is shown in **Figure 7**, although alternative mechanisms have been proposed to occur and most mineralization studies have been performed *in vitro*, such that their conclusions may not necessarily apply to the *in vivo* process. According to the mechanism in **Fig. 7**, Fe(II) ions enter the ferritin molecule through the channels at the three-fold axes, which are known to have metal ion binding sites lined with carboxyl groups (Macara et al., 1973; Stefanini et al., 1989; Treffry et al., 1993; Wardeska et al., 1986). Ferritins molecules endowed with the catalytic

ferroxidase activity (*i.e.*, vertebrate H chains and bacterial ferritins), rapidly oxidize Fe(II) ions to Fe(III) using O_2 or H_2O_2 as an oxidant (Watt et al., 1988; Xu & Chasteen, 1991; Yang & Chasteen, 1999). Further processing of Fe(III) includes movement to the hollow cavity and formation of the mineral core. Ion movements from the ferroxidase site towards the catalytic centres or the protein cavity is driven by an electrostatic potential (Douglas & Ripoll, 1998).

In vertebrate ferritins, L chain subunits are characterized by the presence of five negatively charged Glu residues (Glu57, Glu60, Glu61, Glu64 and Glu67, mouse L-chain numbering), located on the interior surface. These constitute the so-called nucleation sites and are mainly responsible for mineral core formation (Santambrogio et al., 1996). Bacterial ferritins and vertebrate H chains contain some Glu residues equivalent to those in the L chains, which have been suggested to be involved in the nucleation process as well (Bou-Abdallah et al., 2004; Lawson et al., 1991). Overall, the presence of carboxylate groups in both L and H chains is considered to be vital for efficient iron mineralization. As iron incorporation proceeds, Fe(II) oxidation reaction can take place also on the mineral surface formed inside the protein (**Fig. 7**). This reaction becomes predominant as the amount of Fe(II) atoms increases, and when the core is already formed (Bunker et al. 2005).

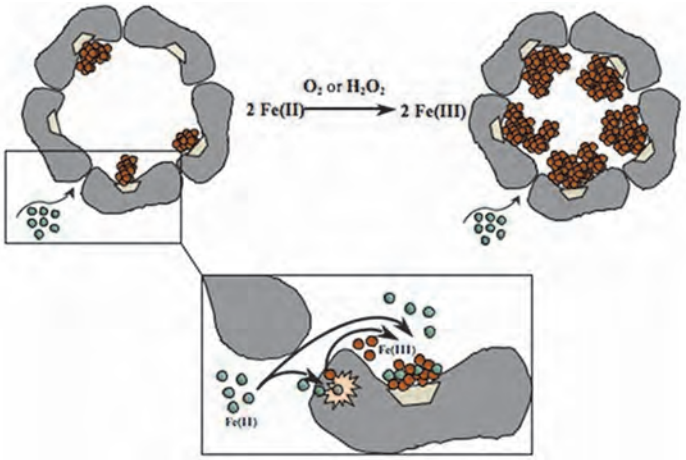

Fig. 7. A schematic illustration of the most widely accepted mechanism for iron incorporation in ferritin proteins. Details are described in the text. Briefly, Fe(II) atoms (green) enter the cavity enclosed by protein subunits (dark grey) *via* the hydrophilic pores. From these pores, Fe(II) atoms are driven to the ferroxidase centre (light pink) where they are oxidized to Fe(III). Fe(III) atoms (brown) move to the iron nucleation sites (light grey), where Fe(III)-mineral formation is initiated. When the Fe(III)-mineral reaches a sufficient size, Fe(II) atoms can also get oxidized directly on the surface of the growing mineral.

As in ferritins, in Dps proteins, after oxidation, iron moves to the protein internal cavity and gives rise to the mineral core. At variance with the ferroxidation step, iron uptake has similar characteristics in both ferritins and Dps proteins. The nucleation step takes place in the internal cavity and is likely to involve specific negative residues (Asp and Glu) lining the Dps internal cavity. Slow nucleation is followed by fast, cooperative growth of the crystal, as shown by the sigmoid kinetics of core formation (Ceci et al., 2010). Cooperativity in the crystal growth step is

modulated by different factors, such as the strength of the electrostatic gradient at the pores, the nature of the oxidant used and ionic strength, which also determine the size distribution of the iron mineral (Bellapadrona et al., 2009; Ceci et al., 2010).

4. Biomimetic synthesis of nanoparticles in ferritins and Dps

NPs of several metal compounds, different from physiological mineral cores and generated using different approaches inside apoferritin or Dps proteins, have been described. These include Fe_3O_4, Co_3O_4, Mn_3O_4, Pt, CoPt, $Cr(OH)_3$, TiO_2, CdS, PbS, CdSe, ZnSe, $CaCO_3$, $SrCO_3$, $BaCO_3$, Pd, Cu, Ag or Au (Bode et al., 2011; Uchida et al., 2010).

Generally, the method used for NPs formation is based simply on the addition of various ions or compounds (simultaneously or sequentially) to apoferritin under specific conditions, allowing the diffusion of the ions or compounds inside the protein shell, followed by an oxidation (using O_2 or H_2O_2 as oxidant) or reduction (generally with $NaBH_4$) step (**Fig. 8**). It is important to notice that most of the mineralization reactions that have been successfully carried out are not specific to iron, suggesting that the electrostatic character of the interior surface of the protein cage is the major player in the mineralization process. Besides the presence of an electrostatic gradient that favours the concentration of cations inside the cavity, it is of great value to have multiple metal binding/nucleation sites able to incorporate efficiently the required metal, which are likely to act as starting points and metal particle seeds for the mineralization reaction (Kasyutich et al., 2010; Ueno et al., 2009). Other parameters have to be taken into account for the preparation of protein-enclosed nanomaterials of biotechnological value, such as: the specific ferritin molecule to be used as a template; the oxidant/reducing agent; and the reaction conditions (*i.e.*, ionic strength, pH, temperature, presence of chelating molecules, etc.).

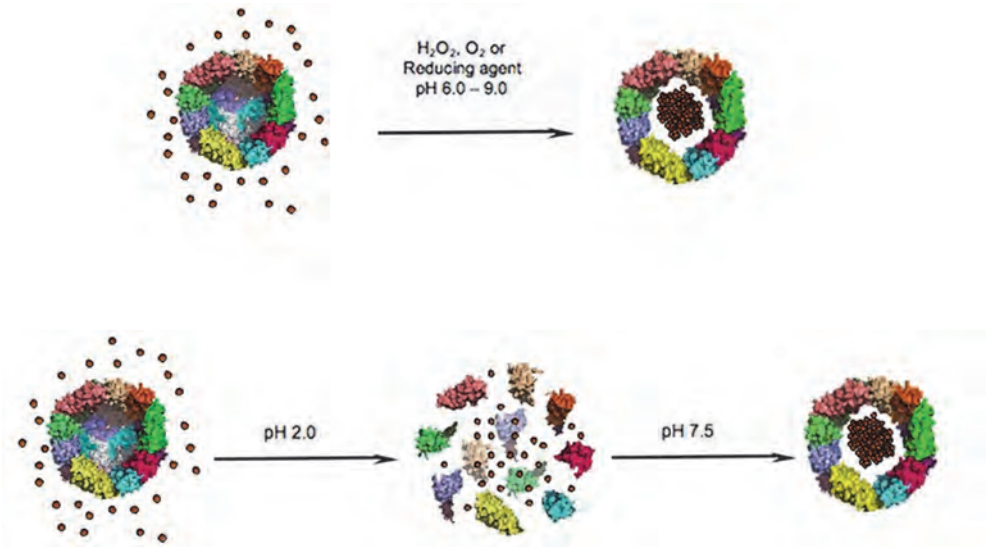

Fig. 8. Schematic illustration of nanoparticles synthesis using ferritins as nano-reactors (see text for details). Top. Ferritin-loading approach. Down. Assembly-disassembly approach.

An alternative approach from the general method described above has been used to incorporate metal particles and other compounds that cannot pass through the ferritin channels. The protein cage has been disassembled in extremely acidic conditions (pH ~2.0) and the desired compounds have been passively encapsulated within the cavity by raising the pH to neutral values (**Fig. 8**) (Yang et al., 2007).

Some of the recent and most significant publications on inorganic nanomaterial synthesis inside the apoferritin cavity are described below, especially in terms of their potential applications in different fields.

4.1 Biomedical applications

Imaging agents are among the compounds that can be successfully loaded within the interior cavity of ferritin proteins. Indeed, Douglas and co-workers have been able to synthesize magnetite NPs encapsulated within the internal cavity of recombinant HuHFt, which possessed T2* MRI properties comparing favourably with known iron oxide MRI contrast agents (*e.g.*, USPIO; Uchida et al., 2008). The same group has hypothesized that ferritins, which often accumulate in human plaques, may serve as an intrinsic vehicle for targeting plaque macrophages (Li et al., 2008), and has demonstrated that modified ferritin cages can be used as fluorescence or MRI agents for *in vivo* detection of vascular macrophages (Terashima et al., 2011).

Two other groups from different laboratories, namely the groups of Aime and of Domınguez-Vera, have prepared water-soluble gadolinium NPs with NMR longitudinal and transverse relaxivities higher than the ones of clinically approved paramagnetic Gd-chelates, thus indicating the great appeal of these novel classes of MRI contrast agents (Geninatti et al., 2006; Sanchez et al., 2009).

A different approach, in terms of the nature of tracer to be used for medical imaging, has been reported (Joh et al., 2011; Lin et al., 2011). Human ferritin has been loaded with radioactive metal ions (^{64}Cu). The ferritin nanotracer thus obtained possessed positron emission tomography (PET) functionalities for high sensitive tumor imaging.

Another potential application of ferritin in the biomedical field has been proposed by Babincová et al. (2000), who suggested to exploit the magnetic properties of the ferritin iron core for magnetic fluid hyperthermia (MFH). MFH is a promising new cancer treatment aimed at burning tumour cells. The procedure has been successfully used in glioma, prostate, liver, and breast tumours. Magnetic NPs should be applied directly to the tumour or injected into the body intravenously and diffuse selectively into cancerous tissues. Adding a safe high-frequency magnetic field (100-400 kHz), leads the particles to heat up, raising the temperature of the tumour cells without damaging the normal ones. However, so far data showing the heating capacity of super-paramagnetic cores encapsulated in ferritins are lacking.

Loading of metal-based drugs inside the ferritin cavity is another appealing opportunity for future tumour therapies. Recently, Xing et al. (2009) successfully encapsulated platinum-based anticancer drugs in the cavity of horse spleen ferritin. The loading capacity of ferritin differed with respect to different drugs but the protein shell remained intact after encapsulation, suggesting that this may be an alternative strategy for the delivery of platinum drugs.

For all the applications described so far, the development of molecules endowed with the ability to specifically target NPs to selected cells and tissues would be of great value. In this

direction, the exterior surface of the ferritin assembly possesses all the features necessary to operate as an appropriate platform for specific cell targeting/delivery. In fact, modification of the exterior surface can be achieved either chemically or genetically. For instance, short peptide sequences and full length antibodies or their fragments, able to recognize specific cell receptors, have been genetically conjugated with the N-terminal region of HuHFt (Uchida et al., 2006 and our unpublished results), or chemically linked to reactive groups on the protein surface (Hainfeld, 1992 and our unpublished results). These findings suggest that cell/tissue specific delivery of imaging and therapeutic agents may be achieved by engineering chemical groups present on the exterior surface of ferritin proteins. Thus, NPs enclosed within HuHFt derivatized with targeting moieties may offer selective delivery possibilities *in vivo*, being presumably non-toxic and biocompatible.

4.2 Catalytic applications

The ferritin cage can serve as a catalytic nanoreactor for chemical reactions promoted by various metal catalysts. In this respect, the spatially restricted inner cavity of ferritin proteins can be exploited as an ideal chemical reaction chamber.

The group of Trevor Douglas has been among the first to investigate the use of ferritin-enclosed iron NPs as photoreduction catalysts (Kim et al., 2002). In particular, the native mineral core encapsulated within the protein cavity, mainly in the ferrihydrite form, has been shown to act as a semiconductor photocatalyst for the reduction of the highly toxic Cr(VI) to the more benign Cr(III). This work has been followed by several papers describing the use of ferritins or Dps proteins, loaded with different metals, in catalytic reactions (Ueno et al., 2004; Suzuki et al., 2009; Prastaro et al., 2009, 2010). The metal catalysts used in the reported organic reactions were generally based on palladium or gold atoms. Chemical reactions such as olefin hydrogenation, Suzuki-Miyaura cross-coupling followed by an enantioselective enzyme-catalyzed reduction to form chiral biaryl alcohols, and homocoupling of boronic acids and potassium aryltrifluoroborates have been described.

4.3 Electronic applications

Ferritin proteins have great potential as building blocks in the fabrication of electronic nanodevices. Yamashita's group has investigated the use of ferritin and Dps-enclosed metal NPs as building units, and has developed the so-called bio-nano process (BNP) for the fabrication of metal oxide semiconductors (MOS), such as floating nanodot gate memory devices or low-temperature polycrystalline silicon thin film transistor flash memories (Hikono et al., 2006; Ichikawa et al., 2007; Miura et al., 2006; Yamashita, 2008). In the BNP ferritin proteins are used as scaffolds to fabricate inorganic nanostructures on structures that are produced by conventional top-down method, such as photolithography. This combination of biological nanofabrication and top-down methods is an attractive process to produce nano-electronic devices. Recently, scientists from the same group have demonstrated that BNP has an advantage in the control of parameters like size, shape, and density of nanodot arrays of MOS devices (Yamada, et al., 2007).

The ability to control the magnetic properties of synthesized NPs is of high importance in the fabrication of magnetic devices on the nanoscale and in their applications. As mentioned above, proteins belonging to the ferritin family provide both a size and shape constrained reaction environment, which allows the magnetic properties of the synthesized magnetic

NPs to be tailored. For example, changing the size of the protein cage (*e.g.*, by switching from ferritins to Dps proteins, or *viceversa*) or the metal loading factor will produce NPs with different size, which might possess different magnetic properties (Gilmore et al., 2005; Klem et al., 2007).

Another approach to control the magnetic properties of ferritin-enclosed NPs consists in the creation of high-order structures based on ferritin cages (Kostiainen et al., 2011). Recombinant ferritins encapsulating Fe_3O_4−γ-Fe_2O_3 iron oxide (magnetoferritin) cores and photodegradable Newkome-type dendrons self-assemble into micron-sized ordered complexes with a face-centred-cubic superstructure. Interestingly, the magnetic properties of magnetoferritin NPs have been shown to be affected directly by the hierarchical organization. Additionally, the magnetoferritin-dendron assemblies efficiently disassembled by a short optical stimulus resulting in the release of free magnetoferritin NPs and restoration of the typical magnetic properties of magnetoferritin.

Protein	PDB ID_chain_Nb of residues (Resolution, Å)	Superimposed residues (Nb)	RMSD (Cα atoms)	Sequence identity (%)
Human L chain ferritin	2FFX_J_173 (1.90)	169	0.57	56
P. furiosus ferritin	2JD7_A_167 (2.80)	158	1.62	31
E. coli Bfr	2Y3Q_A_157 (1.55)	152	2.01	18
L. innocua Dps	1QGH_A_150 (2.35)	125	1.82	10

Table 1. Structure comparison between single subunits of proteins belonging to the ferritin family.

5. Conclusion

In conclusion, in this chapter we have shown that proteins belonging to the ferritin family, and in particular ferritins and Dps proteins, represent a rich and productive set of biomolecular templates for directed materials synthesis in the nano-scale. Indeed, a very wide range of inorganic materials has been successfully synthesized within these cage structures so far. Additionally, the protein shell has been manipulated both chemically and genetically to provide it with new functionalities. As a result, a large variety of materials have been produced, which can be applied in a number of fields as diverse as medicine, chemistry and electronics.

6. Acknowledgment

P.C. thanks the Associazione Italiana per la Ricerca sul Cancro (AIRC), grant agreement n° MFAG10545, for support of the research on biomedical applications of ferritin-based nanoparticles.

The crystal structure of HuHFt (PDB ID: 2CEI, resolution: 1.80 Å, chain A, 172 residues) has been structurally superimposed to the indicated protein subunits using the program "Protein structure comparison service Fold at European Bioinformatics Institute" (PDBeFold; http://www.ebi.ac.uk/msd-srv/ssm/; Krissinel & Henrick, 2004).

7. References

Aisen, P., Enns, C. & Wessling-Resnick, M. (2001) Chemistry and biology of eukaryotic iron metabolism. *Int. J. Biochem.Cell. Biol. Reviews,* 33, 10, 940-959

Alaleona, F., Franceschini, S., Ceci, P., Ilari, A. & Chiancone, E. (2010) Thermosynechococcus elongatus DpsA binds Zn(II) at a unique three histidine-containing ferroxidase center and utilizes O_2 as iron oxidant with very high efficiency, unlike thetypical Dps proteins. *FEBS J.*, 277, 4, 903-917

Almirón, M., Link, A.J., Furlong, D. & Kolter, R. (1992) A novel DNA-binding protein with regulatory and protective roles in starved Escherichia coli. *Genes Dev.*, 6, 12BA, 2646-2654

Andrews, S.C., Arosio, P., Bottke, W., Briat, J.F., von Darl, M., Harrison, P.M., Laulhère, J.P., Levi, S., Lobreaux, S. & Yewdall, S.J. (1992) Structure, function, and evolution of ferritins. *J. Inorg. Biochem.*, 47, 3-4, 161-174

Andrews, S.C., Robinson, A.K. & Rodríguez-Quiñones, F. (2003) Bacterial iron homeostasis. *FEMS Microbiol. Reviews*, 27, 2-3, 215-237

Andrews, S.K. (2010) The Ferritin-like superfamily: Evolution of the biological iron store man from a rubrerythrin-like ancestor. *Biochim. Biophys. Acta*, 1800, 8, 691-705

Babincová, M., Leszczynska, D., Sourivong, P. & Babinec, P. (2000) Selective treatment of neoplastic cells using ferritin-mediated electromagnetic hyperthermia. *Med. Hypotheses,* 54, 2, 177-179

Bellapadrona, G., Stefanini, S., Zamparelli, C., Theil, E.C. & Chiancone, E. (2009) Iron translocation into and out of Listeria innocua Dps and size distribution of the protein-enclosed nanomineral are modulated by the electrostatic gradient at the 3-fold "ferritin-like" pores. *J. Biol. Chem.*, 284, 28, 19101-19109

Bellapadrona, G., Ardini, M., Ceci, P., Stefanini, S. & Chiancone, E. (2010) Dps proteins prevent Fenton-mediated oxidative damage by trapping hydroxyl radicals within the protein shell. *Free Radic. Biol. Med.,* 48, 2,292-297

Bode, S.A., Minten, I.J., Nolte, R.J. & Cornelissen, J.J. (2011) Reactions inside nanoscale protein cages. *Nanoscale,* 3, 6, 2376-2389

Bou-Abdallah, F., Arosio, P., Levi, S., Janus-Chandler, C. & Chasteen, N.D. (2003) Defining metal ion inhibitor interactions with recombinant human H- and L-chain ferritins and site-directed variants: an isothermal titration calorimetry study. *J. Biol. Inorg. Chem.*, 8, 4, 489-497

Bou-Abdallah, F., Biasiotto, G., Arosio, P. & Chasteen, N.D. (2004) The putative "nucleation site" in human H-chain ferritin is not required for mineralization of the iron core. *Biochemistry*, 43, 14, 4332-4337

Bou-Abdallah, F., Zhao, G., Biasiotto, G., Poli, M., Arosio, P. & Chasteen, N.D. (2008) Facilitated diffusion of iron (II) and dioxygen substrates into human H-hain ferritin. A fluorescence and absorbance study employing the ferroxidase center substitution Y34W. *J. Am. Chem. Soc.*, 130, 52, 17801-17811

Braun, V. & Hantke, K. (2011) Recent insights into iron import by bacteria. *Curr. Opin. Chem.. Biol.*, 15, 328–334

Bunker, J., Lowry, T., Davis, G., Zhang, B., Brosnahan, D., Lindsay, S., Costen, R., Choi, S., Arosio, P. & Watt, G.D. (2005) Kinetic studies of iron deposition catalyzed by recombinant human liver heavy and light ferritins and Azotobacter vinelandii bacterioferritin using O_2 and H_2O_2 as oxidants. *Biophys. Chem.*, 114, 2-3, 235-44

Ceci, P., Ilari, A., Falvo, E. & Chiancone, E. (2003) The Dps protein of Agrobacterium tumefaciens does not bind to DNA but protects it toward oxidative cleavage: x-ray crystal structure, iron binding, and hydroxyl-radical scavenging properties. *J. Biol. Chem*., 278, 22, 20319-20326

Ceci, P., Chiancone, E., Kasyutich, O., Bellapadrona, G., Castelli, L., Fittipaldi, M., Gatteschi, D., Innocenti, C. & Sangregorio, C. (2010) Synthesis of iron oxide nanoparticles in Listeria innocua Dps (DNA-binding protein from starved cells): a study with the wild-type protein and a catalytic centre mutant. *Chemistry,* 16, 2, 709-717

Chiancone, E. & Ceci, P. (2010) The multifaceted capacity of Dps proteins to combat bacterial stress conditions: Detoxification of iron and hydrogen peroxide and DNA binding. *Biochim. Biophys. Acta*, 1800, 8, 798-805

Chiaraluce, R., Consalvi, V., Cavallo, S., Ilari, A., Stefanini, S & Chiancone, E. (2000) The unusual dodecameric ferritin from Listeria innocua dissociates below pH 2.0. *Eur. J. Biochem*., 267, 18, 5733-5741

Crichton, R.R. & Boelaert, J.R. (2009) Inorganic Biochemistry of Iron Metabolism from Molecular Mechanisms to Clinical Consequences, 3rd Ed., *John Wiley and Sons, Chichester*, 183–222

Crichton, R.R. & Declercq, J.P. (2010) X-ray structures of ferritins and related proteins. *Biochim. Biophys. Acta*, 1800, 8, 706-718

Crow, A., Lawson, T.L., Lewin, A., Moore, G.R. & Le Brun, N.E. (2009) Structural basis for iron mineralization by bacterioferritin. *J. Am. Chem. Soc*., 131, 19, 6808-6813

Cuypers, M.G., Mitchell, E.P., Romão, C.V. & McSweeney, S.M. (2007) The crystal structure of the Dps2 from Deinococcus radiodurans reveals an unusual pore profile with anon-specific metal binding site. *J. Mol. Biol.,* 371, 3, 787-799

Doig, P., Austin, J.W. & Trust, T.J. (1993) The Helicobacter pylori 19.6-kilodalton protein is an iron-containing protein resembling ferritin. *J. Bacteriol*., 175, 2, 557-560

Douglas, T., & Ripoll, D.R. (1998) Calculated electrostatic gradients in recombinant human H-chain ferritin. *Protein Sci.,* 7, 5, 1083-1091

Drysdale, J.W. (1976) Ferritin phenotypes: structure and metabolism. *Ciba Found Symp*., 9, 51, 41-67

Franceschini, S., Ceci, P., Alaleona, F., Chiancone, E. & Ilari, A. (2006) Antioxidant Dps protein from the thermophilic cyanobacterium Thermosynechococcus elongatus. *FEBS J*., 273, 21, 4913-4928

Frolow, F., Kalb, A.J. & Yariv, J. (1994) Structure of a unique two fold symmetric haem-binding site. *Nat. Struct. Biol*., 1, 7, 453-60

Gálvez, N., Fernández, B., Sánchez, P., Cuesta, R., Ceolín, M., Clemente-León, M., Trasobares, S., López-Haro, M., Calvino, J.J., Stéphan, O. & Domínguez-Vera, J.M. (2008) Comparative structural and chemical studies of ferritin cores with gradual removal of their iron contents. *J. Am. Chem. Soc.,* 25, 130, 8062-8068

Geninatti, C.S., Crich, S., Bussolati, B., Tei, L., Grange, C., Esposito, G., Lanzardo, S., Camussi, G. & Aime, S. (2006) Magnetic resonance visualization of tumor angiogenesis by targeting neural cell adhesion molecules with the highly sensitive gadolinium-loaded apoferritin probe. *Cancer Res.,* 66, 18, 9196-9201

Gilmore, K., Idzerda, Y.U., Klem, M.T., Allen, M., Douglas, T. & Young, M. (2005) Surface contribution to the anisotropy energy of spherical magnetite particles. *J. Appl. Phys*., 97, 10, 10B301 - 10B303

Granier, T., Langlois d'Estaintot, B., Gallois, B., Chevalier, J.M., Précigoux, G., Santambrogio, P. & Arosio, P. (2003) Structural description of the active sites of mouse L-chain ferritin at 1.2 A resolution. *J. Biol. Inorg. Chem*., 8, 1-2, 105-111

Grant, R.A., Filman, D.J., Finkel, S.E., Kolter, R. & Hogle, J.M. (1998) The crystal structure of Dps, a ferritin homolog that binds and protects DNA. *Nat. Struct. Biol*., 5, 4, 294-303

Grünberg, K., Wawer, C., Tebo, B.M., Shüler D. (2001) A large gene cluster encoding several magnetosome proteins is conserved in different species of magnetotactic bacteria. *Appl. Envir. Microbiol.* 67, 10, 4573-4582

Hainfeld, J.F. (1992) Uranium-loaded apoferritin with antibodies attached: molecular design for uranium neutron-capture therapy. *Proc. Natl. Acad. Sci*., 89, 22, 11064-11068

Hikono, T., Matsumura, T., Miura, A., Uraoka, Y., Fuyuki, T., Takeguchi, M., Yoshii, S. & Yamashita, I. (2006) Electron confinement in a metal nanodot monolayer embedded in silicon dioxide produced using ferritin protein, *Appl. Phys. Lett*., 88

Ichikawa, K., Uraoka, Y., Punchaipetch, P., Yano, H., Hatayama, T., Fuyuki, T. & Yamashita, I. (2007) Low-temperature polycrystalline silicon thin film transistor flash memory with ferritin. *Jpn. J. Appl. Phys*., 46, 34, L804-L806

Ilari, A., Stefanini, S., Chiancone, E. & Tsernoglou, D. (2000) The dodecameric ferritin from Listeria innocua contains a novel intersubunit iron-binding site. *Nat. Struct. Biol*., 7, 1, 38-43

Ilari, A., Ceci, P., Ferrari, D., Rossi, G.L. & Chiancone E. (2002) Iron incorporation into Escherichia coli Dps gives rise to a ferritin-like microcrystalline core. *J. Biol. Chem*., 277, 40, 37619-37623

Joh, D.Y., Herman, L.H., Ju, S.Y., Kinder, J., Segal, M.A., Johnson, J.N., Chan, G.K. & Park, J. (2011) On-chip Rayleigh imaging and spectroscopy of carbon nanotubes. *Nano Lett*., 11, 1, 1-7

Johnson, E., Cascio, D., Sawaya, M.R., Gingery, M. & Schröder, I. (2005) Crystal structures of a tetrahedral open pore ferritin from the hyperthermophilic archaeon Archaeoglobus fulgidus. *Structure*, 13, 4, 637-648

Kim, I., Hosein, H.A., Strongin, D.S. & Douglas, T. (2002) Photochemical reactivity of ferritin for Cr (VI) reduction. *Chemistry of Materials*, 14, 4874-4879

Klem, M.T., Resnick, D.A., Gilmore, K., Young M., Idzerda, Y.U. & Douglas, T. (2007) Synthetic control over magnetic moment and exchange bias in all-oxide materials encapsulated within a spherical protein cage. *J. Am. Chem. Soc.*, 129, 1, 197–201

Kauko, A., Pulliainen, A.T., Haataja, S., Meyer-Klaucke, W., Finne, J. & Papageorgiou, A.C. (2006) Iron incorporation in Streptococcus suis Dps-like peroxide resistance protein Dpr requires mobility in the ferroxidase center and leads to the formation of a ferrihydrite-like core. *J. Mol. Biol*., 364, 1, 97-109

Kasyutich, O., Ilari, A., Fiorillo, A., Tatchev, D., Hoell, A. & Ceci, P. (2010) Silver ion incorporation and nanoparticle formation inside the cavity of Pyrococcus furiosus ferritin: structural and size-distribution analyses. *J. Am. Chem. Soc*., 132, 10, 3621-3627

Kostiainen, M.A., Ceci, P., Fornara, M., Hiekkataipale, P., Kasyutich, O., Nolte, R.J.,. Cornelissen, J.J, Desautels, R.D. & van Lierop, J. (2011) Hierarchical Self-Assembly and Optical Disassembly for Controlled Switching of Magnetoferritin Nanoparticle Magnetism. *ACS Nano*, *in press*

Krissinel, E., Henrick, K. (2004) Secondary-structure matching (SSM), a new tool for fast protein structure alignment in three dimensions. *Acta Crystallogr D Biol Crystallogr.* 60, 2256-2268

Lawson, D.M., Artymiuk, P.J., Yewdall, S.J., Smith, J.M., Livingstone, J.C., Treffry, A., Luzzago, A., Levi, S., Arosio, P., Cesareni, G. & et al. (1991) Solving the structure of human H-ferritin by genetically engineering intermolecular crystal contacts. *Nature,* 349, 541–544

Lawson, D.M., Treffry, A., Artymiuk, P.J., Harrison, P.M., Yewdall, S.J., Luzzago, A., Cesareni, G., Levi, S. & Arosio, P. (1989) Identification of the ferroxidase centre in ferritin. *FEBS Lett.,* 254, 1-2, 207-210

Le Brun, N.E., Crow, A., Murphy, M.E., Mauk, A.G. & Moore, G.R. (2010) Iron core mineralisation in prokaryotic ferritins. *Biochim Biophys Acta,* 1800, 8, 732-744.

Li, W., Xu, L.H., Forssell, C., Sullivan, J.L. & Yuan, X.M. (2008) Overexpression of transferring receptor and ferritin related to clinical symptoms and destabilization of human carotid plaques. *Exp. Biol. Med.,* 233, 7, 818-826

Lin, X., Xie, J., Niu, G., Zhang, F., Gao, H., Yang, M., Quan, Q., Aronova, M.A., Zhang, G., Lee, S., Leapman, R. & Chen, X. (2011) Chimeric ferritin nanocages for multiple function loading and multimodal imaging. *Nano Lett*., 11, 2, 814-819

Liu, H-l., Zhou, H.N., Xing, W.M., Zhao, J.F., Li, S.X., Huang, J.F. & Bi, R.C. (2004) 2.6 A resolution crystal structure of the bacterioferritin from Azotobacter vinelandii. *FEBS Lett*., 573, 1-3, 93-98

Liu, X. & Theil, E.C. (2005) Ferritins: dynamic management of biological iron and oxygen chemistry. *Acc. Chem. Res.,* 38, 3, 167-175

Lewin, A., Moore, G.R. & Le Brun, N.E. (2005) Formation of protein-coated iron minerals. *Dalton Trans*., 22, 3597–3610

Macara, I.G., Hoy, T.G. & Harrison, P.M. (1973) The formation of ferritin from apoferritin. Inhibition and metal ion-binding studies. *Biochem. J*., 135, 4, 785-789.

Mann, S., Spark, N.H.C., Board, R.G. (1990) Magnetotactic Bacteria: microbiology, biomineralization, palaeomagnetism and biotechnology. *Adv. Microbiol. Physiol.,* 31, 125-181.

Massover, W.H. & Cowley, J.M. (1973) The ultrastructure of ferritin macromolecules. The lattice structure of the core crystallites. *Proc. Natl. Acad. Sci U.S*., 70, 12, 3847-3851

McCord, J.M. & Fridovich, I. (1988) Superoxide dismutase: the first twenty years (1968-1988). *Free Radic. Biol. Med*., 5, 5-6,363-369

Miura, A., Hkono, T., Matsumura, T., Yano, H., Hatayama, T., Uraoka, Y., Fuyuki, T., Yoshii, S. & Yamashita I. (2006) Floating nanodot gate memory devices based on biomineralized inorganic nanodot array as a storage node. *Jpn. J. Appl. Phys*., 45, L1–L3

Nordlund, P. & Eklund, H. (1995) Di-iron-carboxylate proteins. *Curr. Opin. Struct. Biol. Reviews*, 5, 6, 758-766

Prastaro, A., Ceci, P., Chiancone, E., Boffi, A., Cirilli, R., Colone, M., Fabrizi, G., Stringaro, A. & Cacchi, S. (2009) Suzuki-Miyaura cross-coupling catalyzed by protein-stabilized palladium nanoparticles under aerobic conditions in water: application to a one-pot chemoenzymatic enantioselective synthesis of chiral biaryl alcohols. *Green Chemistry,* 11, 1929-1932

Prastaro, A., Ceci, P., Chiancone, E., Boffi, A., Fabrizi, G.& Cacchi, S. (2010) Homocoupling of arylboronic acids and potassium aryltrifluoroborates catalyzed by protein-stabilized palladium nanoparticles under air in water. *Tetrahedron Letters,* 51, 18, 2550-2552

Ren, B., Tibbelin, G., Kajino, T., Asami, O. & Ladenstein, R. (2003) The multi-layered structure of Dps with a novel di-nuclear ferroxidase center. *J. Mol. Biol*., 329, 3, 467-477

Rohrer, J.S., Islam, Q.T., Watt, G.D., Sayers, D.E. & Theil, E.C. (1990) Iron environment in ferritin with large amounts of phosphate, from Azotobacter vinelandii and horse spleen, analyzed using extended X-ray absorption fine-structure (EXAFS). *Biochemistry*, 29, 1, 259–264

Romão, C.V., Regalla, M., Xavier, A.V., Teixeira, M., Liu, M.Y. & Le Gall, J.A. (2000) Bacterioferritin from the strict anaerobe Desulfovibrio desulfuricans ATCC 27774. *Biochemistry*, 39, 23, 6841-6849

Romão, C.V., Mitchell, E.P. & McSweeney, S. (2006) The crystal structure of Deinococcus radiodurans Dps protein (DR2263) reveals the presence of a novel metal centre in the N terminus. *J. Biol. Inorg. Chem.*, 11, 7, 891-902

Sánchez, P., Valero, E., Gálvez, N., Domínguez-Vera, J.M., Marinone, M., Poletti, G., Corti, M. & Lascialfari, A. (2009) MRI relaxation properties of water-soluble apoferritin-encapsulated gadolinium oxide hydroxide nanoparticles. *Dalton Trans.*, 7, 5, 800-804.

Santambrogio, P., Levi, S., Cozzi, A., Corsi, B. & Arosio, P. (1996) Evidence that the specificity of iron incorporation into homopolymers of human ferritin L- and H-chains is conferred by the nucleation and ferroxidase centres. *Biochem. J.*, 314, Pt 1, 139-144.

Stefanini, S., Desideri, A., Vecchini, P., Drakenberg, T. & Chiancone, E. (1989) Identification of the iron entry channels in apoferritin. Chemical modification and spectroscopic studies. *Biochemistry,* 28, 1, 378-382

Stefanini, S., Cavallo, S., Montanini, B. & Chiancone E. (1999) Incorporation of iron by the unusual dodecameric ferritin from Listeria innocua. *Biochem. J.,* 338, Pt 1, 71-75

Stillman, T.J., Hempstead, P.D., Artymiuk, P.J., Andrews, S.C., Hudson, A.J., Treffry, A., Guest, J.R. & Harrison, P.M. (2001) The high-resolution X-ray crystallographic structure of the ferritin (EcFtnA) of Escherichia coli; comparison with human H ferritin (HuHF) and the structures of the Fe(3+) and Zn(2+) derivatives. *J. Mol. Biol.*, 307, 2, 587-603

Suzuki, M., Abe, M., Ueno, T., Abe, S., Goto, T., Toda, Y., Akita, T., Yamada, Y. & Watanabe,Y. (2009) Preparation and catalytic reaction of Au/Pd bimetallic nanoparticles in apo-ferritin. *Chem Commun.* (*Camb),* 32, 4871-4873

Tatur, J., Hagen, W.R. & Matias, P.M. (2007) Crystal structure of the ferritin from the hyperthermophilic archaeal anaerobe Pyrococcus furiosus. *J. Biol. Inorg. Chem.*, 12, 5, 615-630

Terashima, M., Uchida, M., Kosuge, H., Tsao, P.S., Young, M.J., Conolly, S.M., Douglas, T. & McConnell, M.V. (2011) Human ferritin cages for imaging vascular macrophages. *Biomaterials*, 32, 5, 1430-1437

Toussaint, L., Bertrand, L., Hue, L., Crichton, R.R. & Declercq, J.P. (2007) High-resolution X-ray structures of human apoferritin H-chain mutants correlated with their activity and metal-binding sites. *J. Mol. Biol.*, 365, 2, 440-452

Treffry, A., Bauminger, E.R., Hechel, D., Hodson, N.W., Nowik, I., Yewdall, S.J. & Harrison, P.M. (1993) Defining the roles of the threefold channels in iron uptake, iron oxidation and iron-core formation in ferritin: a study aided by site-directed mutagenesis. *Biochem. J.*, 296, Pt 3, 721-728

Trikha, J., Theil, E.C. & Allewell, N.M. (1995) High resolution crystal structures of amphibian red-cell L ferritin: potential roles for structural plasticity and solvation in function. *J. Mol. Biol.*, 248, 5, 949-967

Uchida M., Flenniken, M.L., Allen, M., Willits, D.A., Crowley, B.E., Brumfield, S., Willis, A.F., Jackiw, L., Jutila, M., Young, M.J. & Douglas, T. (2006) Targeting of cancer cells with ferrimagnetic ferritin cage nanoparticles. *J. Am .Chem. Soc.*, 128, 51, 16626-16633

Uchida, M., Terashima, M., Cunningham, C.H., Suzuki, Y., Willits, D.A., Willis, A.F., Yang, P.C., Tsao, P.S., McConnell, M.V., Young, M.J. & Douglas, T. (2008) A human ferritin iron oxide nano-composite magnetic resonance contrast agent. *Magn. Reson. Med*., 60, 5, 1073-1081

Uchida, M., Kang, S., Reichhardt, C., Harlen, K. & Douglas, T. (2010) The ferritin superfamily: Supramolecular templates for materials synthesis. *Biochim. Biophys. Acta*, 1800, 8, 834-845

Ueno, T., Suzuki, M., Goto, T., Matsumoto, T., Nagayama, K. & Watanabe, Y. (2004) Size-selective olefin hydrogenation by a Pd nanocluster provided in an apo-ferritin cage. *Angew. Chem. Int. Ed.*, 43, 19, 2527-2530

Ueno, T. Abe, M., Hirata, K., Abe, S., Suzuki, M., Shimizu, N., Yamamoto, M., Takata, M. & Watanabe, Y. (2009) Process of accumulation of metal ions on the interior surface of apo-ferritin: crystal structures of a series of apo-ferritins containing variable quantities of Pd (II) ions *J. Am. Chem. Soc*., 131, 14, 5094-5100

Wardeska, J.G., Viglione, B. & Chasteen, N.D. (1986) Metal ion complexes of apoferritin. Evidence for initial binding in the hydrophilic channels. *J. Biol. Chem.,* 261, 15, 6677-6683

Watt, G.D., Jacobs, D. & Frankel, R.B. (1988) Redox reactivity of bacterial and mammalian ferritin: is reductant entry into the ferritin interior a necessary step for iron release? *Proc. Natl. Acad. Sci U S A*, 85, 20, 7457-7461

Xing, R., Wang, X., Zhang, C., Zhang, Y., Wang, Q., Yang, Z. & Guo, Z. (2009) Characterization and cellular uptake of platinum anticancer drugs encapsulated in apoferritin. *J. Inorg. Biochem.,* 103, 7, 1039-1044

Xu, B. & Chasteen, N.D. (1991) Iron oxidation chemistry in ferritin. Increasing Fe/O_2 stoichiometry during core formation. *J. Biol. Chem.*, 266, 30, 19965-19970

Yang, X. & Chasteen, N.D. (1999) Ferroxidase activity of ferritin: effects of pH, buffer and Fe (II) and Fe(III) concentrations on Fe(II) autoxidation and ferroxidation. *Biochem. J.,* 338, Pt 3, 615-618

Yang, Z., Wang, X., Diao, H., Zhang, J., Li, H., Sun, H. & Guo, Z. (2007) Encapsulation of platinum anticancer drugs by apoferritin. *Chem. Commun. (Camb.)*, 7, 33, 3453-3455

Yamamoto, Y., Poole, L.B., Hantgan, R.R. & Kamio, Y. (2002) An iron-binding protein, Dpr, from Streptococcus mutans prevents iron-dependent hydroxyl radical formation in vitro. *J. Bacteriol.*, 184, 11, 2931-2939

Yamada, K., Yoshii, S., Kumagai, S., Miura, A., Uraoka, Y., Fuyuki, T. & Yamashita, I. (2007) Effects of dot density and dot size on charge injection characteristics in nanodot array produced by protein supramolecules, *Jpn. J. Appl. Phys.,* 46, 7549–7553

Yamashita, I. (2008) Biosupramolecules for nano-devices: biomineralization of nanoparticles and their applications. *J. Mater. Chem*., 18, 3813–3820

Zanotti, G., Papinutto, E., Dundon, W., Battistutta, R., Seveso, M., Giudice, G., Rappuoli, R. & Montecucco, C. (2002) Structure of the neutrophil-activating protein from Helicobacter pylori. *J. Mol. Biol*., 323, 1, 125-130

Pymol (Delano Scientific LLC, San Carlos, LA; http://www.pymol.org)